# Developments in the understanding and modeling of the agglomeration of suspended crystals in crystallization from solutions

René David, Fabienne Espitalier, Ana Cameirao, Loïc Rouleau

# Developments in the Understanding and Modeling of the Agglomeration of Suspended Crystals in Crystallization from Solutions†

**René David[1], Fabienne Espitalier[1] and Ana Cameirão[1]**
*Laboratory for Chemical Engineering of Particulate Solids*
**Loïc Rouleau[2]**
*Institut Français du Pétrole*

**Abstract**

*The paper deals with the modeling of the agglomeration of crystals during their crystallization. Crystal agglomeration actually consists of two steps, i.e. particle collision and agglomerate strengthening by crystal growth. The expression of agglomeration rates can be written in terms of a collision rate coupled with an efficiency factor. However, the mechanisms and rates of collision and disruption are related to the type of liquid flow that the mother crystals and the agglomerate experience, which in turn are dependent on their respective sizes. In particular, the influences of the absolute and relative sizes of mother particles, of the local energy dissipation and of the fluid viscosity differ according to the three types of motions, i.e. Brownian, laminar, turbulent. Besides this, the rapidity of the crystal growth, which in turn is a function of the supersaturation, plays a major role in the strengthening rate. The question of the limit cases between two regimes is also treated. The method takes into account and unifies previous expressions obtained by other authors in the various regimes. The model is also able to calculate the average agglomeration degrees.*

*The paper is illustrated by one example of crystal agglomeration from our recent work and introduces a general model.*

## 1. Introduction

The structure of many crystalline compounds obtained from suspension crystallization shows the presence of agglomerated crystallites or crystals. Solid bridges between the mother crystals bind the agglomerates. In some cases, the shape of the particles suggests a multistage agglomeration process with primary and secondary agglomerates (**Fig. 1a**). The sizes of the final agglomerates (1 μm to 1 mm) and of their sub-units (a few tenths of nm to a few tenths of μm) are widely spread out, depending on both the nature of the crystalline compound and the crystallization process. Among other materials, such structures have been observed for zeolites [1,21], adipic acid [2], calcium carbonate (calcite) and calcium oxalate monohydrate [3,12], pseudo-boehmite [4], barium titanate [5].

Since the original paper of Schmoluchowski [20] one hundred years ago, many authors have tackled these mechanisms (see for instance [6,7]), and more recent progress [3,8,9] has been made in the simple and comprehensive modeling of agglomeration. In fact, crystal agglomeration consists of two steps, i.e. particle collision and agglomerate strengthening.

In the following paper, we intend to present a unified approach of the agglomeration in crystallization, which relies partly on published models that account for the different processes, which are applicable to the different size ranges and in agreement with experimental observations.

## 2. Efficiency of a binary agglomeration during crystallization

We suppose that all agglomerations result from a binary collision (**Fig. 1b**).

[1] CNRS-Ecole des Mines d'Albi-Carmaux, F-81013 Albi

Two particles of respective sizes $S_i$ and $S_j \leq S_i$ collide. An intermediate labile aggregate is formed. The collision of rate $r_{col}$ is followed either by disruption into the two former mother particles or by consolidation by crystallization into an agglomerate, with respective rates $r_d$ and $r_{con}$.

We suppose that the disruption and consolidation processes depend only on the concentration of the labile intermediate aggregate, which is assumed to be in a quasi-equilibrium state. Thus,

$$r_{col}=r_d+r_{con} \text{ with } r_{con}=k_{con}C_{int} \text{ and } r_d=k_dC_{int} \qquad (1)$$

From the above set of equations (1), we derive the overall agglomeration rate

$$r_a=r_{con}=\eta r_{col} \qquad (2)$$

Where $\eta$ is the efficiency of the agglomeration, defined in terms of rate constants or characteristic times

$$\eta=1/(1+k_d/k_{con})=1/(1+t_{cr}/t_d) \qquad (3)$$

We assume that the consolidation process is crystallization: crystalline bridges are built by crystalline growth between the particles. Marchal et al [8] have shown that the crystallization time may be expressed as a function of the growth rate G of the crystal

$$t_{cr}=S_j f(S_j,S_j)/G \quad \text{and thus} \quad \eta = 1/(1+S_j f(S_j,S_j)/Gt_d) \qquad (4)$$

The function f accounts for relative sizes and its value always ranges between 10.5 and 12 from the expression of Marchal et al. [8]: It may be considered as a constant.

The variety of the sizes of the final agglomerates (1 µm to 1 mm) obtained in crystallization and of their sub-units (a few tenths of nm to a few tenths of µm) is large. When compared with the characteristic sizes of fluid mechanics in the liquid phase (Taylor, Kolmogoroff, and Batchelor microscales [10]), it is clear that multiple collision and disruption mechanisms occur which are related to the type of liquid flow that the mother crystals and the intermediate aggregate experience. On the other hand, it is likely that the consolidation mechanism is crystalline growth. Its rate ranges between $10^{-6}$ and $10^{-11}$ m/s [11]. One difficulty is that the crystal growth rate varies during the process as a consequence of the depletion of the solute in the liquid phase.

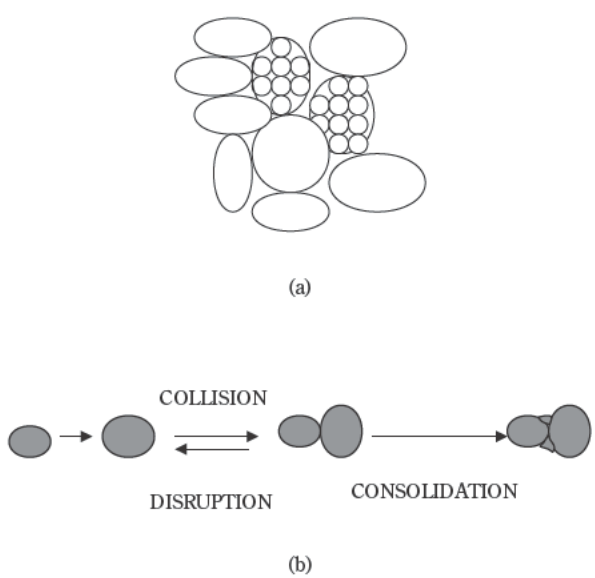


**Fig. 1** Shape and creation of a two-stage agglomerate.

## 3. Different regimes of particle motion

In the following paper, we assume that the agglomeration takes place under three different types of motion – Brownian, laminar, and turbulent – depending on the size of the colliding particles and of the resulting agglomerate. The collision between particles from size classes j and $i \geq j$ is assumed to take place under motion k=b,l,t and the labile aggregate to be exposed to motion k′. Thus, the expressions of $r_{col,k}$, $t_{d,k'}$ and consequently $\eta_{j,i,k'}$ will be different according to the types of fluid motions governing the collision and the disruption.

(a) Particles smaller than the Batchelor scale $l_B$ experience Brownian motion: Particles collide as a result of a diffusion process. The random disruption competes with crystallization.

(b) Particles between $l_B$ and the Kolmogoroff scale $l_K$ are subjected to the laminar stretching and swirling process, also called engulfment [10]. The shear stress accounts for disruption, which competes with crystallization.

(c) Finally, particles larger than $l_K$ collide under the influence of fluctuating velocities and are disrupted by the same phenomenon [8]. Crystallization is also here the agglomerating process.

If both mother particles and the agglomerate fall under one single regime, the values of k and k′ are obvious.

The simplest exception is when the intermediate aggregate becomes larger than the upper limit of the regime governing collision of the mother particles. Then, k′ switches over to the regime for larger parti-

cles.

This is not the case if the mother particles experience different regimes due to their very different sizes. Therefore, we have to make the following assumptions. The collision of particles in the Brownian and laminar regimes is governed by the diffusion of the smaller particle to the surface of the larger one (k=b). The same approach holds for Brownian-turbulent collisions in the laminar boundary layer. The intermediate aggregate then evolves under a laminar disruption regime (k′=l), the smaller particle being protected by the boundary layer of the larger one.

Collisions between particles in the laminar and in the turbulent ranges are consecutive to the turbulent motion (k=t). The intermediate aggregate evolves like a turbulent agglomerate because its size exceeds $l_K$ (k′=t).

The different possibilities are summarized in **Fig. 2**.

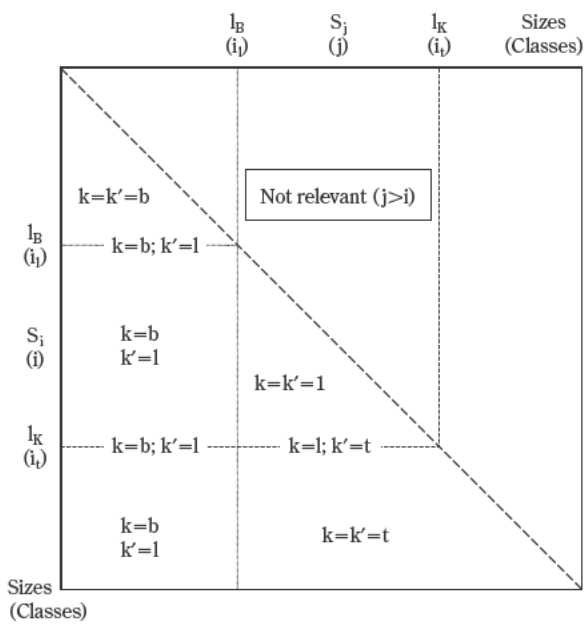


**Fig. 2** Different types of collisions and consolidation processes of agglomerates as a function of the sizes of the mother particles.

## 4. Expressions of agglomeration kernels

The agglomeration rate in the collision regime k and in the disruption regime k′ is expressed as

$$r_{a,j,i,k,k'}=\eta_{j,i,k'}r_{col,j,i,k} \quad (5)$$

It is generally accepted since the work of Schmoluchowski [20] that

$$r_{col,j,i,k}=\beta_{c,j,i,k}\,N_i\,N_j \quad (6)$$

where $N_i$ and $N_j$ are the respective concentrations of particles belonging to the classes i and j, respectively. Thus,

$$r_{a,j,i,k,k'}=\eta_{j,i,k'}\beta_{c,j,i,k}\,N_i\,N_j=\beta_{j,i,k,k'}\,N_i\,N_j \quad (7)$$

**Table 1** presents the expressions of $\beta_{c,j,i,k}$ and $\eta_{j,i,k'}$ for the different values of k and k′ for either rapid or slow growth rates. In the case of a slow crystal growth rate, Eq. (4) simplifies to

$$\eta_{j,i,k'}\sim Gt_d/S_j \quad (8)$$

However, this simplification may not be correct for very small, i.e. nanometric sizes $S_j$. In this case, the entire expression (4) should be kept for $\eta_{j,i,k'}$.

The expressions for the Brownian and laminar collision kernels have been established and discussed since many years [6,7,9,24] (**Table 1**). In the Brownian range, when the particles are free of electric charges, Van der Waals forces ensure the cohesion of aggregates until crystallization takes place [22]; Otherwise, the DLVO theory [9] accounts for coagulation processes, but collisions with a third particle may lead to releases in the case of low crystalline growth.

Marchal [8] has proposed expressions for both collision rate and efficiency in the turbulent regime, which were validated on adipic acid. More recently, Hounslow and co-workers introduced several expressions for the laminar agglomeration efficiency [12]; among them we have retained the most recent one, which is in agreement with our general formulation of section 2. The disruption time is then expressed as [12]

$$t_d=\sigma^*L/[A_l\rho_{susp}PX] \quad (9)$$

where X has the dimension of a length; Several expressions combining $S_i$ and $S_j$ have been tried for X and this will be discussed later. P is the dissipated energy per unit mass of suspension, $\rho_{susp}$ is the density of the suspension, $\sigma^*$ is the tensile strength of the solid, $L$ a contact length between particles, $A_l$ a dimensionless constant.

A first point is that the efficiency $\eta_{j,i,k'}$ is close to 1 for the Brownian and laminar disruption regimes if the growth rate is high.

Now, let us have a closer look at the different types of collisions in **Fig. 2** under a low (**Table 2**) or high (**Table 3**) crystalline growth rate. In order to check the parameter sensitivity, we have examined three

**Table 1** Expressions of collision rate constant and consolidation efficiency for either low or high growth rates. Example of stirred tanks.

| | LOW GROWTH RATE | HIGH GROWTH RATE |
|---|---|---|
| **k** | **Collision rate constant $\beta_{c,j,i,k}$** | |
| b | $=\frac{2k_BT}{3\mu}\frac{(S_i+S_j)^2}{S_iS_j}$ (1) | |
| l | $=k'_{Al}\frac{(S_i+S_j)^3P^{1/2}}{v^{1/2}}$ with $k'_{Al}\#0.16$ (2) | |
| t | $=k'_{At}(S_i+S_j)^2ND_A$ [8] (3) | |
| **k′** | **Efficiency $\eta_{j,i,k'}$** | |
| b | $=1/(1+A_bS_j/G)$ (4) | $=1$ |
| l | $=\frac{G\sigma^*L}{A_lP\rho_{susp}XS_j}$ with $L\sigma^*/A_l\approx1$ [12] (5) | $=1$ |
| t | $=\frac{G\left(1-\left(\frac{S_i+S_j}{\lambda_c}\right)^2\right)}{A_tNS_j}$ [8] (6) | $=\frac{1}{1+\frac{S_j}{Gt_d}}$ with $t_d=\frac{\left(1-\left(\frac{S_i+S_j}{\lambda_c}\right)^2\right)}{A_tN}$ [8] (7)* |

* $\lambda_c$ is the Taylor scale in the suspension, generally in the order of magnitude of a few mm and $\sim P^{-1/2}$.

**Table 2** Influence of stirring speed N or dissipated energy P, sizes of mother particles $S_j$ and $S_i$ on collision rate constant and efficiency for different size ranges of mother particles and agglomerate. Case of low growth rates.

| $S_j$ | $S_i$ | $S_a$ | k | k′ | LOW GROWTH RATE | Collision rate constant $\beta_{c\,j,i,k}$ | Agglomeration efficiency $\eta_{j,i,k'}$ | Overall agglomeration rate constant $\beta_{j,i,k,k'}$ |
|---|---|---|---|---|---|---|---|---|
| $\le l_B$ | $\le l_B$ | $\le l_B$ | b | b | Expressions | (1) | (4) | (1) × (4) |
| | | | | | N or P increases | – | – | – |
| | | | | | $S_j=S_i$ increases | Constant$=8kT/3\mu$ | Decreases | Decreases |
| | | | | | $S_j$ increases with constant $S_i$ | Decreases | Decreases $\sim S_j^{-1}$ | Decreases |
| $\le l_B$ | Any size $\ge S_j$ | $> l_B$ | b | l | Expressions | (1) | (5) | (1) × (5) |
| | | | | | N or P increases | – | Decreases $\sim P^{-1}$ | Decreases $\sim P^{-1}$ |
| | | | | | $S_j=S_i$ increases | Constant$=8kT/3\mu$ | Decreases $\sim S_i^{-2}$ | Decreases $\sim S_i^{-2}$ |
| | | | | | $S_j$ increases with constant $S_i$ | Decreases | Decreases $\sim S_j^{-2}$ | Decreases |
| $> l_B$ $\le l_K$ | $> l_B$ $\le l_K$ | $> l_B$ $\le l_K$ | l | l | Expressions | (2) | (5) | (2) × (5) |
| | | | | | N or P increases | Increases $\sim P^{1/2}$ | Decreases $\sim P^{-1}$ | Decreases $\sim P^{-1/2}$ |
| | | | | | $S_j=S_i$ increases | Increases $\sim S_i^3$ | Decreases $\sim S_i^{-2}$ | Increases $\sim S_i$ |
| | | | | | $S_j$ increases with constant $S_i$ | Increases | Decreases $\sim S_j^{-2}$ | Decreases |
| $> l_B$ $\le l_K$ | $> l_B$ $\le l_K$ | $> l_K$ | l | t | Expressions | (2) | (6) | (2) × (6) |
| | | | | | N or P increases | Increases $\sim P^{1/2}$ | Decreases $\sim P^{-1/3}$ | Increases $\sim P^{1/6}$ |
| | | | | | $S_j=S_i$ increases | Increases $\sim S_i^3$ | Decreases $\sim S_i^{-1}$ | Increases $\sim S_i^2$ |
| | | | | | $S_j$ increases with constant $S_i$ | Increases | Decreases $\sim S_j^{-1}$ | Minimum at $S_j=S_i/2$ |
| $> l_K$ | $> l_K$ | $> l_K$ | t | t | Expressions | (3) | (6) | (3) × (6) |
| | | | | | N or P increases | Increases $\sim P^{1/3}$ | Decreases $\sim P^{-1/3}$ | – , but decreases with sizes close to the Taylor scale |
| | | | | | $S_j=S_i$ increases | Increases $\sim S_i^2$ | Decreases $\sim S_i^{-1}$ | Increases $\sim S_i$, until the Taylor scale is reached |
| | | | | | $S_j$ increases with constant $S_i$ | Increases | Decreases $\sim S_j^{-1}$ | Decreases |

The relations numbered (1)-(7) correspond to those of **Table 1**.

**Table 3** Influence of stirring speed N or dissipated energy P, sizes of mother particles $S_j$ and $S_i$ on collision rate constant and efficiency for different size ranges of mother particles and agglomerate. Case of high growth rates.

| $S_j$ | $S_i$ | $S_a$ | k | k′ | **HIGH GROWTH RATE** | Collision rate constant $\beta_{c\,j,i,k}$ | Agglomeration efficiency $\eta_{j,i,k'}$ | Overall agglomeration rate constant $\beta_{j,i,k,k'}$ |
|---|---|---|---|---|---|---|---|---|
| $\leq l_B$ | $\leq l_B$ | $\leq l_B$ | b | b | Expressions | (1) | | (2) |
| | | | | | N or P increases | – | | – |
| | | | | | $S_j=S_i$ increases | Constant$=8kT/3\mu$ | | Constant$=8kT/3\mu$ |
| | | | | | $S_j$ increases with constant $S_i$ | Decreases | | Decreases |
| $\leq l_B$ | Any size $\geq S_j$ | $>l_B$ | b | 1 | Expressions | (1) | | (2) |
| | | | | | N or P increases | – | | – |
| | | | | | $S_j=S_i$ increases | Constant$=8kT/3\mu$ | $=1$ | Constant$=8kT/3\mu$ |
| | | | | | $S_j$ increases with constant $S_i$ | Decreases | | Decreases |
| $>l_B$ $\leq l_K$ | $>l_B$ $\leq l_K$ | $>l_B$ $\leq l_K$ | 1 | 1 | Expressions | (2) | | (2) |
| | | | | | N or P increases | Increases $\sim P^{1/2}$ | | Increases $\sim P^{1/2}$ |
| | | | | | $S_j=S_i$ increases | Increases $\sim S_i^3$ | | Increases $\sim S_i^3$ |
| | | | | | $S_j$ increases with constant $S_i$ | Increases | | Increases |
| $\leq l_K$ | $\leq l_K$ | $>l_K$ | 1 | t | Expressions | (2) | (7) | (2)×(7) |
| | | | | | N or P increases | Increases $\sim P^{1/2}$ | Decreases | Increases |
| | | | | | $S_j=S_i$ increases | Increases $\sim S_i^3$ | Decreases | Increases |
| | | | | | $S_j$ increases with constant $S_i$ | Increases | Decreases | ? |
| $>l_K$ | $>l_K$ | $>l_K$ | t | t | Expressions | (3) | (7) | (3)×(7) |
| | | | | | N or P increases | Increases $\sim P^{1/3}$ | Decreases | Increases, but diminishes when Taylor scale is reached |
| | | | | | $S_j=S_i$ increases | Increases $\sim S_i^2$ | Decreases | Increases, but diminishes when Taylor scale is reached |
| | | | | | $S_j$ increases with constant $S_i$ | Increases | Decreases | ? |

The relations numbered (1)-(7) correspond to those of **Table 1**.

influences: The increase of power dissipated in the suspension, the increase of size for the agglomeration of particles of the same size ($S_i=S_j$), and the increase of smaller particle sizes $S_j$ at a constant large particle size $S_i$. As far as the dissipated power P is concerned, note that (a) there is no influence of P on $\beta_{i,i,k,k'}$ for mixing in the Brownian regime, (b) that high power is less favorable to laminar agglomeration at low growth rates, whereas (c) it has an enhancing factor at high growth rates. Finally, there is a miscellaneous influence of P on the agglomeration kernel in the turbulent regime.

The variation of the collision rate constant $\beta_{c,i,i,k}$, the efficiency $\eta_{i,i,k'}$ and the agglomeration kernel $\beta_{i,i,k,k'}$ in the case of colliding particles of equal sizes is particularly interesting (**Figs. 3** and **4**): $\beta_{c,i,i,k}$ increases continuously with increasing size, whereas $\eta_{i,i,k'}$ always decreases. The kernel is an increasing function of size for high growth rates and shows a mini-

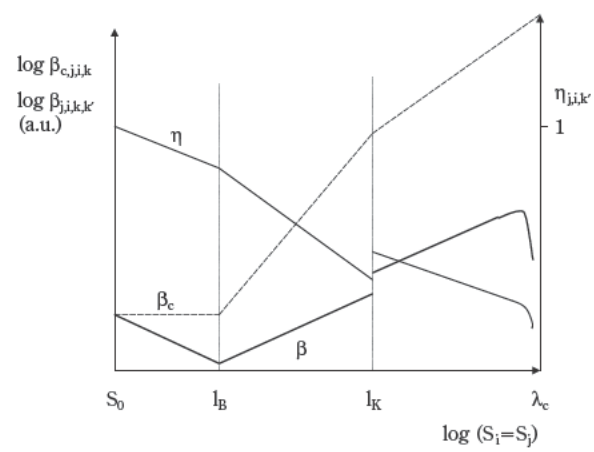


**Fig. 3** Collision and overall agglomeration rate constant against the common size of mother particles for collision of particles of the same size. Case of very low growth rates.

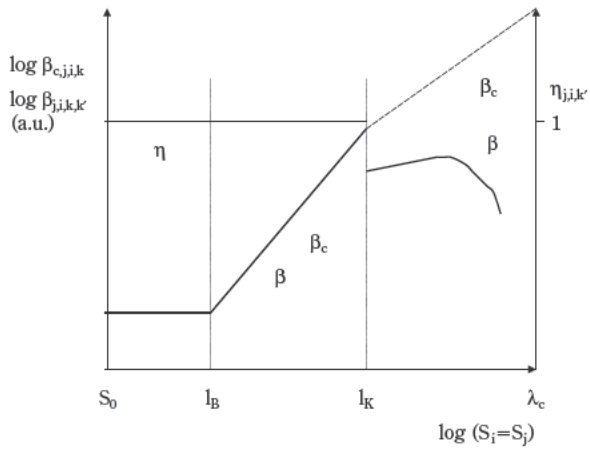


**Fig. 4** Collision and overall agglomeration rate constant against the common size of mother particles for collision of particles of the same size. Case of high growth rates.

mum value at size $l_B$ at low growth rates. In all cases, both $\eta_{i,i,k'}$ and $\beta_{i,i,k,k'}$ tend towards zero when the size reaches the turbulent Taylor scale $\lambda_c$ [8].

Finally, looking at the influence of relative particle sizes, **Tables 2** and **3** show a major difference between the shapes of agglomerates generated by high and low growth rates in the different regimes. If the agglomeration kernel decreases with increasing $S_j/S_i$ it means that the agglomeration between small and large particles is favored. Conversely, if the kernel increases it means that agglomeration between particles of similar sizes is enhanced. Thus, in the first case, agglomerates show the so-called "snowball" effect (compact agglomerates made from agglomerates and elementary smaller particles or agglomerates), while in the second case, the agglomerates will be made from equally sized mother agglomerates.

For high growth rates, the first case prevails until the Batchelor microscale is reached and the second case seems likely above this scale. At low growth rates, the kernel behaves differently: The limit between the two cases is about the Kolmogoroff microscale.

Generally, one should notice the different and sometimes opposite trends predicted by the model for the different couples of mother particles depending on their absolute and relative sizes and the intensity of the growth rate. This may explain the discrepancies observed in the literature [8,12,13] when trying to report and to model the variations of the agglomeration rate for several crystallizations or several crystal size ranges and varying the stirring power.

## 5. Transition between Brownian and laminar regimes

The transition occurs at the size limit $l_B$, which may be calculated as follows. The significance of the Batchelor scale is underlined by Baldyga and Bourne [10]. When a fluid portion undergoes laminar stretching, it reaches a reduced transversal size which is so small that the transportation length of a molecule by diffusion or of a particle due to Brownian motion during the stretching time is of the same order of magnitude as the thickness of the laminae. This length scale is called the Batchelor scale [10].

$$l_B=\left(\frac{\nu D^2}{P}\right)^{1/4} \tag{10}$$

where the diffusivity D of a particle of size $S_j$, the most mobile of the two, is [23]

$$D=\frac{k_B T}{3\pi\mu S_j} \tag{11}$$

$\mu$ and $\nu$ are the dynamic and kinematic viscosities of the suspension, respectively; $l_B$ is in the order of magnitude of a few hundred nm for particles from 10 to 100 nm in stirred tanks. Note that the collision rates calculated by (1) and (2) in **Table 1** are of the same order of magnitude when sizes of colliding particles both equal $l_B$. Therefore, since the collision rate increases strongly with the size of particles in the laminar regime, we assume that the representative curves cross at $S_j=l_B$ (**Figs. 3** and **4**). For the low growth rates, we have no indication that the efficiencies are equal at the transition size. But, the physical continuity seems a fair assumption for the agglomeration process, as a change of slope (**Figs. 3** and **4**) will rapidly make the laminar agglomeration rate predominant with increasing sizes.

## 6. Transition between laminar and turbulent regimes

The Kolmogoroff microscale is expressed as [10]

$$l_K=(\nu^3/P)^{1/4} \tag{12}$$

If two particles are smaller than the Kolmogoroff microscale, they experience no velocity fluctuations for both collision and disruption. This scale is in the order of magnitude of some tenths of micrometers. An equality of the collision and agglomeration rate expressions seems likely at $l_K$, but the slope of the collision rate is reduced when switching to the turbulent regime (**Figs. 3** and **4**).

## 7. Particle size distribution

The modeling is based on the method of classes introduced by David et al. [2,8,14] where the size scale of particles is divided into $n_c$ classes, and where the limits of these classes are in geometric progression with a factor of $2^{1/3}$ [10], i.e. a factor of 2 for the volumes. $n_c$ is chosen in order to verify $L_{n_c} > \lambda_c$. The actual continuous distribution is replaced by a virtual discrete distribution which works with classes of rank n, whose average size is $S_n = (L_n + L_{n-1})/2$ and where the shape factor is volumetrically the same. Recently, Verkoeijen et al. [26] presented a generalized volume approach of population balances in the same manner which was applied to comminution, sintering and granulation. Here, the impact on class n of agglomerations between particles of classes j and $i \geq j$ is represented by stoichiometric coefficients $\nu_{n,j,i}$ by analogy with a chemical reaction system. These coefficients have to be calculated in order

(a) to balance the solid volume, which is equivalent to the conservation of the 3rd moment of the distribution, and,

(b) to remove one single particle for each agglomeration (except for agglomeration (i,i) where only 1/2 a particle disappears due to symmetry) to permit compliance with the 0th moment equation of the PSD.

Three different schemes of agglomeration have to be differentiated with respect to the relative sizes of the particles. Hereafter, **(i)** represents the particle class i and so on

$$1/2\ \mathbf{(i)} + 1/2\ \mathbf{(i)} \rightarrow 1/2\ \mathbf{(i+1)} \tag{13}$$

$$\mathbf{(i-1)} + 1/2\ \mathbf{(i)} \rightarrow 1/2\ \mathbf{(i+1)} \tag{14}$$

$$v_i/(v_i - v_j)\ \mathbf{(j<i-1)} + \mathbf{(i)} \rightarrow v_i/(v_i - v_j)\ \mathbf{(i)} \tag{15}$$

The corresponding stoichiometric coefficients that stand for the impact of agglomeration (i,j) on particle class n are

$$\nu_{n,i,i} = \delta_{n,i+1}/2 - \delta_{n,i} \tag{16}$$

$$\nu_{n,i-1,i} = \delta_{n,i+1}/2 - \delta_{n,i}/2 - \delta_{n,i-1} \tag{17}$$

$$\nu_{n,j,i} = v_j/(v_i - v_j)\delta_{n,i} - v_i/(v_i - v_j)\delta_{n,j} \tag{18}$$

$\delta_{n,i}$ is an element of the Kronecker matrix ($\delta_{n,i}=0$ if $n \neq i$ and $\delta_{n,i}=1$ if $n=i$). The resulting agglomeration rate for class n is

$$R_{A,k,k',n} = \sum_{i=1}^{n_c} \sum_{j=1}^{i} \nu_{n,j,i} r_{a,j,i,k,k'} = \sum_{i=1}^{n_c} \sum_{j=1}^{i} \nu_{n,j,i} \beta_{j,i,k,k'} N_j N_i \tag{19}$$

The particle size distribution (PSD) $\Psi$ is integrated over class n between sizes $L_{n-1}$ and $L_n$ for $n_c \geq n \geq 1$ in a batch stirred crystallizer with suspension volume $V_{susp}$, yielding the particle concentration in class n, i.e. $N_n$

$$\frac{1}{V_{susp}} \frac{d(N_n V_{susp})}{dt} = G(L_{n-1})\Psi(L_{n-1}) - G(L_n)\Psi(L_n) + \delta_{n,1} r_N + \sum_{k=b;1;t} \sum_{k'=b;1;t} R_{A,k,k',n} \tag{20}$$

with $\Psi(L_{-1}) = \Psi(L_{n_c}) = 0$. Note that $r_N$ is the generation rate of crystalline particles. The nucleation term accounts for the generation of crystallites in class 1 only.

Classical characteristic length scales are derived from the discrete distribution; For instance

$$\overline{L_{43}} = \frac{\sum_{n=1}^{n_c} S_n^4 N_n}{\sum_{n=1}^{n_c} S_n^3 N_n} \tag{21}$$

The total number of particles per suspension volume unit which disappeared by an agglomeration through mechanism (k,k′) is

$$R_{A,k,k',T} = \sum_{n=1}^{N_c} R_{A,k,k',n} \tag{22}$$

The rate of molar production of crystalline solid mass per unit volume of suspension is expressed as

$$\frac{dc_c}{dt} = \Phi_v \frac{\rho_s}{M_s} \left( 3G \sum_{n=1}^{n_c} L_n^2 N_n + S_0^3 r_N \right) \tag{23}$$

where $\Phi_v$ is a volumetric shape factor, $\rho_s$ and $M_s$ are the density and molar mass of the solid, respectively, and $r_N$ is the nucleation rate of the crystalline solid.

There may be other types of solids with concentration $c_s$, for instance amorphous solids, in the crystallizer. The concentration of the solute $c_l$ can be derived from the solute plus solid mass balance

$$(c_{s0} + c_{c0}) V_{susp} + c_{l0} V_{l0} = (c_c + c_s) V_{susp} + c_l V_l \tag{24}$$

$$\text{With } V_l = V_{susp}(1 - M_s c_s/\rho_s + M_C c_C/\rho_C) \tag{25}$$

Finally, the growth rate is related to the supersaturation $\sigma = c_l/C_c^* - 1$

$$G = G_0 \sigma^{k_1} \tag{26}$$

## 8. Implementation of other agglomerate properties

The description of agglomerates cannot simply be elucidated by means of a size distribution. The ag-

glomerate structure has to be characterized by other variables such as shape factors, porosity, fractality, or agglomeration degrees. The purpose of this section is to show how our method can give access to the average values of such additional properties, without introducing a 2-variable distribution function like that used by [15,16].

Therefore, we simply look at how each property is modified – or not – by every elementary agglomeration (i,j). In this section, we use the example of two different agglomeration degrees which we define as follows:

We call a primary agglomerate a structure made of crystallites with a minimum size $L_{PA}$ which is approximated by the boundary between class $n_{PA}$ and $n_{PA}+1$. The primary agglomeration degree (=average number of crystallites in the primary agglomerates) is

$$\overline{n_{PA}} = \frac{N_{CT} - \sum_{A=1}^{n_{PA}} N_n 2^{n-1}}{N_{PA}} \tag{27}$$

where $N_{CT}$ and $N_{PA}$ are the total concentration of crystallites and primary agglomerates, respectively.

In an earlier paper [14], we used another definition for the agglomeration degree. Starting from $N_0$ particle concentration at time 0, and since every agglomeration removes one model particle from the suspension, we added the total number of agglomerations in the k regime for collision and the k′ regime for consolidation

$$\overline{n_{PA1}} = \frac{1}{1 + \int_0^t R_{A,k,k',T}\,dt} \tag{28}$$

This relation encompasses all agglomerations in the regimes k and k′ without any minimal size of the resulting agglomerate.

Similarly, the secondary agglomeration degree is the number of primary agglomerates embedded in a secondary agglomerate

$$\overline{\overline{n_{SA}}} = \frac{(N_{PA} - N_{FPA})}{N_{SA}} \tag{29}$$

where $N_{FPA}$ and $N_{SA}$ are the total concentration of free primary agglomerates and secondary agglomerates, respectively.

Both definitions correspond to quantities which are easy to observe via image analysis with SEM or ESEM pictures.

**Table 4** shows the stoichiometric coefficients affecting $N_{PA}$, $N_{FPA}$ and $N_{SA}$ for all elementary agglomeration processes between our classes of virtual particles.

Note that $N_{CT}$ is not affected by any agglomeration. It only depends on the nucleation rate and is expressed in a batch crystallizer as

$$\frac{dN_{CT}}{dt} = r_N \tag{30}$$

Consequently, the equations describing the evolu-

**Table 4** Stoichiometric coefficients for primary agglomerates, free primary agglomerates, secondary agglomerates concentrations depending on the type of agglomeration: (i) represents the $i^{th}$-class of particles. Free primary agglomerates are only encountered in class $n_{PA}+1$. The standard virtual agglomerate of class $n \geq n_{PA}+1$ encompasses $2n-n_{PA}-1$ primary agglomerates.

| Agglomerations | Stoichiometric coefficients for | | |
|---|---|---|---|
| | $N_{PA}$ | $N_{FPA}$ | $N_{SA}$ |
| $v_i/(v_i-v_j)(1\leq j\leq i-2)+(1\leq i\leq n_{PA}) \longrightarrow v_i/(v_i-v_j)(i\leq n_{PA})$ | 0 | 0 | 0 |
| $(n_{PA}-1)+1/2(n_{PA}) \longrightarrow 1/2(n_{PA}+1)$ | 1/2 | 1/2 | 0 |
| $1/2(n_{PA})+1/2(n_{PA}) \longrightarrow 1/2(n_{PA}+1)$ | 1/2 | 1/2 | 0 |
| $(n_{PA})+1/2(n_{PA}+1) \longrightarrow 1/2(n_{PA}+2)$ | 1/2 | −1/2 | 1/2 |
| $1/2(n_{PA}+1)+1/2(n_{PA}+1) \longrightarrow 1/2(n_{PA}+2)$ | 0 | −1 | 1/2 |
| $(n_{PA}+1)+1/2(n_{PA}+2) \longrightarrow 1/2(n_{PA}+3)$ | 0 | −1 | 0 |
| $v_i/(v_i-v_j)(j=n_{PA}+1)+(i\geq n_{PA}+3) \longrightarrow v_i/(v_i-v_j)(i)$ | 0 | $-v_i/(v_i-v_j)$ | $v_j/(v_i-v_j)$ |
| $v_i/(v_i-v_j)(n_{PA}+2\leq j\leq i-2)+(n_{PA}+4\leq i\leq n_c) \longrightarrow v_i/(v_i-v_j)(i)$ | 0 | 0 | −1 |
| $(i-1)+1/2\ (i\geq n_{PA}+3) \longrightarrow 1/2(i+1)$ | 0 | 0 | −1 |
| $1/2(i\geq n_{PA}+2)+1/2(i) \longrightarrow 1/2(i+1)$ | 0 | 0 | −1/2 |

tions of $N_{PA}$, $N_{FPA}$ and $N_{SA}$ against time are

$$\frac{dN_{FPA}}{dt}=G(L_{PA})\Psi(L_{PA})+\frac{1}{2}[r_{a,n_{PA}-1,n_{PA},k,k'}+r_{a,n_{PA},n_{PA},k,k'}-r_{a,n_{PA},n_{PA}+1,k,k'}]-r_{a,n_{PA}+1,n_{PA}+1,k,k'}-r_{a,n_{PA}+1,n_{PA}+2,k,k'}-\sum_{i=n_{PA}+3}^{n_c}\frac{v_i}{(v_i-v_{n_{PA}+1})}r_{a,n_{PA}+1,i,k,k'}$$

$$\frac{dN_{PA}}{dt}=G(L_{PA})\Psi(L_{PA})+\frac{1}{2}[r_{a,n_{PA}-1,n_{PA},k,k'}+r_{a,n_{PA},n_{PA},k,k'}+r_{a,n_{PA},n_{PA}+1,k,k'}]$$

$$\frac{dN_{SA}}{dt}=\frac{1}{2}[r_{a,n_{PA},n_{PA}+1,k,k'}+r_{a,n_{PA}+1,n_{PA}+1,k,k'}]-\sum_{i=n_{PA}+3}^{n_c}\frac{v_{n_{PA}+1}}{(v_i-v_{n_{PA}+1})}r_{a,n_{PA}+1,i,k,k'}-\sum_{i=n_{PA}+3}^{n_c}\sum_{j=n_{PA}+2}^{i-1}r_{a,j,i,k,k'}-\frac{1}{2}\sum_{i=n_{PA}+2}^{n_c}r_{a,i,i,k,k'} \quad (31)$$

The $G\Psi$ term in differential equations for $N_{PA}$ and $N_{FPA}$ accounts for the growth of the agglomerate from class $n_{PA}$ into class $n_{PA}+1$, thus leading to a free primary agglomerate according to our definition. Conversely, the quality of the agglomerate or free primary agglomerate is not lost by the growth from class $n_{PA}+1$ into class $n_{PA}+2$. In the same manner, secondary agglomerates cannot be generated by simple growth from primary agglomerates, but only via an agglomeration of primary agglomerates: Therefore, there is no $G\Psi$ term in the differential equation for $N_{SA}$.

Such sets of equations can be derived for other average properties such as, for instance, porosity: One simply has to express how far every agglomeration changes the porosity of the agglomerates.

## 9. Example of amorphous crystallization coupled with agglomeration of the crystalline form

The model is applied to the crystallization of zeolites. In this type of crystallization, an amorphous gel is formed immediately after mixing the reactants [1,17]. This gel is poured into a batch crystallizer and heated at temperatures ranging between 80 and 250°C, at which point the amorphous solid transforms into a less soluble, crystalline solid [25].

Experimental details are available in [23]. Samples were taken from the solid and the liquid phases in order to determine the crystallinity by XRD, the PSD by laser diffractometry, and supersaturation by atomic absorption spectroscopy.

The following observations were made:

(a) The crystallizer is mechanically stirred (axial stirrer with a power number of 1 and diameter $D_A$=0.08 m). At temperatures of around 200°C, the suspension behaves from a rheological point of view like a Newtonian fluid with a kinematic viscosity close to $10^{-6}$ $m^2.s^{-1}$, and a suspension density of about $10^3$ $kg.m^{-3}$.

(b) Amorphous particles in the suspension have an initial concentration of $N_0$ and an initial size of $L_0$=65 nm ($S_0$=57.5 nm).

(c) The suspension volume of $10^{-2}$ $m^3$ is constant. Coupled with the following assumptions:

(d) The initial supersaturation in the liquid phase is

$$\sigma_0 = C^*_{am}/C_c^*-1 \quad (32)$$

(e) The increase of the solid mass during the whole process due to crystal growth can be neglected.

(f) According to the literature [18], it is likely that the crystallites are nucleated by the surface transformation of the amorphous particles. Agglomeration starts as soon as the external surface is crystalline. Dissolution of the amorphous compound obeys a Gaussian rate law. This is consistent with our experimental XRD observations when monitoring the crystalline fraction of the solid [19]. The molar concentration of the amorphous compound am decreases according to

$$\frac{dc_s}{dt}=\frac{dc_{am}}{dt}=-\Phi_v\frac{\rho_s}{M_s}S_0^3 r_N \quad (33)$$

(g) The crystal growth is independent of crystal size. Its order is $k_1$=1 with respect to supersaturation.

(h) An amorphous particle has the same density $\rho_s$, shape factor $\Phi_v$, and molecular weight $M_s$ as a crystalline one. No agglomerate porosity was assumed.

(i) Agglomeration takes place via the mechanisms described above.

(j) The laminar to turbulent transition occurs at about 100 to 70 μm (Kolmogorov microscale) and agglomeration stops at 3.5 to 2.5 mm (Taylor microscale) depending on the stirring speed ($N$=1.7−4.3 $s^{-1}$). As the observed agglomerates are smaller than 50 μm, we assume that there is no turbulent agglomeration taking place.

(k) For the sake of simplicity, we will choose in the following $L_{PA}=l_B$, i.e. $n_{PA}=m$.

The above equation system is expressed in dimen-

sionless variables: time $\theta=tG_0/L_0$ with $G=G_0\,\sigma^{k_1}$ (G is estimated from SEM micrographies of crystallites by taking samples at different times); reduced size $\lambda=L/L_0$; reduced average class size $s=S/L_0$; reduced particle concentration in class n: $y_n=N_n/N_0$; reduced density distribution $\Phi=\Psi L_0/N_0$; reduced concentration in the liquid phase $x_l=c_l/C_c^*$; reduced supersaturation $\sigma=c_l/C_c^*-1$; reduced concentration of the amorphous solid phase $x_a=c_a/C_c^*$; and reduced concentration of the crystalline solid phase $x_c=c_c/C_c^*$.

## 10. Results, parameter estimation and discussion

Then, the initial conditions of the differential equations are

$$y_n=0\,(n=1,n_c);\ y_{CT}=y_{PA}=y_{FPA}=y_{SA}=0;\quad x_a=x_{a0}=m_0/c^*;\ x_{c0}=0 \tag{34}$$

Four dimensionless parameters remain: the initial fraction of the solid phase

$$m_0=m_{tot}/(\rho_s V_{susp})=\Phi_v S_0^3 N_0 \tag{35},$$

the initial supersaturation $\sigma_0$, the solubility

$$c^*=M_s C_c^*/\rho_s \tag{36}$$

and the Brownian agglomeration rate constant

$$K_{Ab}=2k_B T L_0 N_0/(3\mu G_0)=2k_B T m_0/(3\mu G_0 \Phi_v s_0^3 L_0^2) \tag{37}$$

Then, the dimensionless agglomeration rate from (36) and Eqs. (1) and (4) of **Table 1** is expressed as

$$r_{a,j,i,b,b}\frac{N_0L_0}{G_0}=K_{Ab}\frac{(s_i+s_j)^2}{s_i s_j}\frac{1}{1+\left(\frac{A_bL_0}{G_0}\right)\frac{s_j}{\sigma_0^{k_1}}} \tag{38}$$

$A_b$ was estimated at about $10^{-6}$ $s^{-1}$ by equalizing the agglomeration rates in the laminar and in the Brownian regimes at $l_B=S_i=S_j$. The efficiency was always very close to 1 and, therefore, the simulations were not sensitive to $A_b$.

The reduced laminar collision rate constant $K_{Al}$ can be deduced from $k'_{Al}$ by

$$K_{Al}=k'_{Al}(P/\nu)^{1/2}L_0/G_0 \tag{39}$$

Normally, $k'_{Al}$ should be equal to 0.16 according to the literature [9].

The initial upper size $L_0$ and the kinetic growth rate constant $G_0$ were estimated from the SEM pictures of the crystallites, with the actual supersaturation known. However, such a determination for $G_0$ is rather inaccurate. Therefore, it is checked by comparing the reduced final time of complete supersaturation consumption $\theta_F$ and the measured one $t_FG_0/L_0$. The parameters $m_0$, $c^*$ and $\sigma_0$ are deduced from the measured solid mass and the initial and final concentrations of the solute in the liquid phase. No indication could be found in the literature about the order $k_1$ in the crystal growth rate expression for the type of zeolite studied. Therefore, the simplest way was to take $k_1=1$.

Finally, two parameters were fitted by trial and error. Several expressions of X were tried in the expression of the laminar efficiency factor (**Table 1**). The best fit with the experimental PSD was observed using $X=S_i$. In accordance with [12], the term $\sigma^*L/A_l$ should be fixed at 1, which is the value for calcite, but $\sigma^*$ and $L$ may vary from species to species and from polymorph to polymorph. Finally, the best fit was obtained with $\sigma^*L/A_l=0.0035$.

Thus,

$$r_{a,j,i,l,l}\frac{N_0L_0}{G_0}=K_{Al}\frac{m_0}{\Phi_v s_0^3}(s_i+s_j)^3\frac{1}{1+\left(\frac{A_lP\rho_{susp}L_0^2}{G_0\sigma^*L}\right)\frac{s_js_i}{\sigma_0^{k_1}}} \tag{40}$$

A comparison between the final experimental and the calculated particle size distributions, both with the same geometrical progression for the class sizes on the abscissa scale, is represented in **Fig. 5**. The experimental PSD was obtained from samples taken by laser diffraction analysis. The agreement is fair with respect to the particular shape of the experimental PSD. The values of experimental parameters of the simulation are listed in **Table 5**. However, the main peak of the PSD is narrower for the simulation than

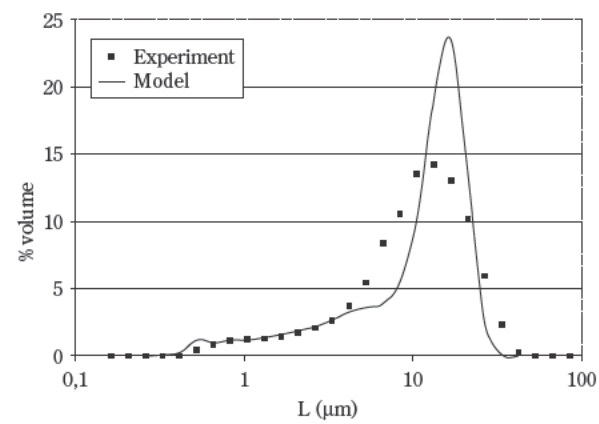


**Fig. 5** Comparison of experimental and calculated PSD. Experimental conditions: T=180°C; N=2.92 $s^{-1}$; stirrer power number=1; stirrer diameter=0.08 m; for other parametric values see **Table 5**.

Table 5 Values of parameters of the simulation presented in Fig. 5.

| | |
|---|---|
| P= | $8.16\times10^{-3}$ W/kg |
| ν= | $10^{-6}$ m².s$^{-1}$ |
| $V_{susp}$= | $10^{-2}$ m³ |
| $\rho_{susp}$= | 1000 kg.m$^{-3}$ |
| $\rho_{sm}=\rho_c$ | 1800 kg.m$^{-3}$ |
| $M_{sm}=M_c$ | 7.1 kg.mol$^{-1}$ |
| $k_1$= | 1 |
| $L_0$= | 65 nm |
| $G_0$= | $2.5\times10^{-11}$ m.s$^{-1}$ |
| $m_0$= | $m_{tot}/(\rho_s V_{susp})=0.048$ |
| $K_{Ab}$= | $2k_BTm_0/(3\mu G_0\Phi_v s_0^3 L_0^2)=8.36\times10^6$ |
| $K_{Al}$= | $k'_{Al}(P/\nu)^{1/2}L_0\, m_0/(\Phi_v s_0^3 G_0)$ with $k'_{Al}=0.16$ |
| c*= | $C^*M_c/\rho_c=0.01$ |
| $\sigma_0$= | =0.55 |
| $A_b$= | $=10^{-4}$ s$^{-1}$ |
| $A_l/\sigma^*L$= | =0.0035 Pa$^{-1}$.m$^{-1}$[12] |

the experimental one. The porosity (0.35-0.5) shown by the secondary agglomerates (primary agglomerates appear non-porous) on SEM pictures may explain this difference: the agglomerates generated by laminar collision and consolidation processes, and whose size was measured by the laser diffraction, show an apparent volume larger than the actual solid volume. Due to the fractal nature of these agglomerates, an overall size dispersion is expected to be registered by the laser diffractometer.

## 11. Conclusions

The binary agglomeration of crystalline particles in a supersaturated solution has been shown to be the combination of two independent processes, i.e. particle collision and aggregate consolidation. Therefore, the overall agglomeration rate is expressed as the collision rate times an efficiency factor. This efficiency relies on a competition between crystallization and disruption.

When multiple agglomeration is evidenced, both collision and consolidation may take place in a Brownian, laminar or turbulent regime, depending on the size of the mother and daughter particles. In stirred tanks, the dependence on parameters such as stirring speed, liquid viscosity, or particle size differs according to the regimes involved. Boundary rules for limit cases have been established.

The method takes into account and unifies previous expressions obtained by other authors in the various regimes and checked by them with respect to experimental results for several agglomerating products.

As far as the structure of agglomerates is concerned, the model using a reaction-like set of stoichiometric equations was able to calculate the average primary and secondary agglomeration degrees.

An example based on zeolite crystallization from the amorphous state has been developed. The particle size distribution was found to be in very good agreement with the experimental one.

We plan to extend the present work to other products that are subject to multiple agglomeration and other crystal properties.


## Acknowledgements

The authors thank the Institut Français du Pétrole for scientific and financial support of this work.


## Nomenclature

| | | |
|---|---|---|
| $A_b$ | : Brownian efficiency constant | [s$^{-1}$] |
| $A_l$ | : Laminar efficiency constant | [−] |
| $A_t$ | : Turbulent efficiency constant | [m$^3$.s$^{-1}$] |
| $c$,$C$ | : Concentrations | [mol.m$^{-3}$] |
| $c^*$ | : Reduced solubility | [−] |
| $C^*$ | : Solubility | [mol.m$^{-3}$] |
| $D_A$ | : Stirrer diameter | [m] |
| $D$ | : Diffusivity of a particle | [m$^2$.s$^{-1}$] |
| $f$ | : Marchal's [8] function | [−] |
| $G$ | : Growth rate of a crystal | [m.s$^{-1}$] |
| $G_0$ | : Growth rate constant | [m.s$^{-1}$] |
| $k_B$ | : Boltzmann Constant | [Jmolecule$^{-1}$K$^{-1}$] |
| $k'_{Al}$ | : Constant of collision rate constant for laminar regime | [−] |
| $k'_{At}$ | : Constant of collision rate constant for turbulent regime | [−] |
| $k_d$ | : Disruption rate constant | [−] |
| $k_{con}$ | : Consolidation rate constant | [−] |
| $k_l$ | : Kinetic order of growth rate | [−] |
| $k_B$ | : Boltzmann Constant | [J.molecule$^{-1}$.K$^{-1}$] |
| $K_{Ak}$ | : Agglomeration rate constant of type $k$ | [−] |
| $l_K$ | : Kolmogorov microscale | [m] |
| $l_B$ | : Batchelor scale | [m] |
| $L$ | : Particle size | [m] |
| $L_0$ | : Amorphous particle size | [m] |
| $\overline{L_{43}}$ | : Average final particle size | [m] |
| $m_0$ | : Initial fraction of solid phase | [−] |
| $m_{tot}$ | : Initial particle mass | [kg] |
| $M_s$ | : Solid molar mass | [kg.mol$^{-1}$] |
| $N$ | : Stirring speed | [s$^{-1}$] |

| | | |
|---|---|---|
| $n_c$ | : Total size class number | [−] |
| $\overline{n_{PA}}$ | : Primary agglomeration degree | [−] |
| $\overline{n_{PAI}}$ | : Primary agglomeration degree | [−] |
| $\overline{n_{SA}}$ | : Secondary agglomeration degree | [−] |
| $N_0$ | : Particle concentration at time 0 | [$m^{-3}$] |
| $N_{CT}$ | : Total concentration of crystallites | [$m^{-3}$] |
| $N_{FPA}$ | : Total concentration of free primary agglomerates | [$m^{-3}$] |
| $N_{PA}$ | : Total concentration of primary agglomerates | [$m^{-3}$] |
| $N_n$ | : Concentration of particles belonging to the class $n$ | [$m^{-3}$] |
| $N_{SA}$ | : Total concentration of secondary agglomerates | [$m^{-3}$] |
| $P$ | : Dissipated power per unit mass | [$W.kg^{-1}$] |
| $r_a$ | : Overall agglomeration rate | [$m^{-3}.s^{-1}$] |
| $r_d$ | : Disruption rate for two particles $i$ and $j$ | [$m^{-3}.s^{-1}$] |
| $r_{col}$ | : Collision rate for two particles $i$ and $j$ | [$m^{-3}.s^{-1}$] |
| $r_{con}$ | : Consolidation rate for two particles $i$ and $j$ | [$m^{-3}.s^{-1}$] |
| $r_N$ | : Nucleation rate | [$m^{-3}.s^{-1}$] |
| $R_{A,k,k',n}$ | : Agglomeration rate of class $n$ | [$m^{-3}.s^{-1}$] |
| $R_{A,k,k',T}$ | : Global agglomeration rate for agglomeration of type $k,k'$ | [$m^{-3}.s^{-1}$] |
| $s_i$ | : Reduced average size | [−] |
| $S_i$ | : Class average size= $(L_{i-1}+L_i)/2$ | [m] |
| $t$ | : Time | [s] |
| $t_{cr}$ | : Crystallisation time | [s] |
| $t_d$ | : Disruption time | [s] |
| $t_F$ | : Measured final time of consumption | [s] |
| $T$ | : Temperature | [K] |
| $V$ | : Volume | [$m^3$] |
| $V_{susp}$ | : Suspension volume | [$m^3$] |
| v | : Particle volume | [$m^3$] |
| $X$ | : Length parameter (see Eq. (9)) | [m] |
| $x$ | : Reduced concentration in the suspension | [−] |
| $y_n$ | : Reduced particle concentration in class $n$ | [−] |
| $\beta_{c,j,i,k}$ | : Collision rate constant for type $k$ | [$m^3.s^{-1}$] |
| $\beta_{j,i,k,k'}$ | : Agglomeration rate constant for type $k,k'$ | [$m^3.s^{-1}$] |
| $\delta_{n,i}$ | : Element of the Kronecker matrix | [−] |
| $\eta$ | : Efficiency of the agglomeration | [−] |
| $\Phi$ | : Reduced particle size density function (PSD) | [−] |
| $\Phi_v$ | : Volumetric shape factor | [−] |
| $\lambda$ | : Reduced particle size | [−] |
| $\lambda_c$ | : Taylor microscale | [m] |
| $\mu$ | : Dynamic viscosity of suspension | [$kg.m^{-1}s^{-1}$] |
| $\upsilon$ | : Kinematic viscosity of suspension | [$m^2.s^{-1}$] |
| $\upsilon_{n,j,i}$ | : Stoichiometric coefficient accounting for the impact of agglomeration $(j,i)$ on particle class $n$ | [−] |
| $\rho_c$ | : Crystal density | [$kg.m^{-3}$] |
| $\rho_s$ | : Solid density | [$kg.m^{-3}$] |
| $\rho_{susp}$ | : Suspension density | [$kg.m^{-3}$] |
| $\psi$ | : Particle size density function (PSD) | [$m^{-4}$] |
| $\sigma$ | : Supersaturation | [−] |
| $\sigma_0$ | : Initial supersaturation | [−] |
| $\sigma^*$ | : Yield stress | [Pa] |
| $\theta$ | : Reduced time | [−] |
| $\theta_F$ | : Reduced final time of complete supersaturation consumption | [−] |

### Subscripts and superscripts

| | |
|---|---|
| $a/A$ | : Agglomeration |
| $am$ | : Amorphous |
| $c$ | : Crystal |
| $col$ | : Collision |
| $con$ | : Consolidation |
| $cr$ | : Growth |
| $CT$ | : Total crystallites |
| $d$ | : Disruption |
| $F$ | : Final |
| $FPA$ | : Free primary agglomerates |
| $i,j,n$ | : Class |
| $l$ | : Liquid |
| $N$ | : Nucleation |
| $k$ | : Regime for collision |
| $k'$ | : Regime for consolidation |
| $PA$ | : Primary agglomerates |
| $s$ | : Solid |
| $SA$ | : Secondary agglomerates |
| $susp$ | : Suspension |
| $T$ | : Total |
| $0$ | : Initial |
| * | : Equilibrium |

## BIBLIOGRAPHY


[1] Barrer, R.M.: Hydrothermal Chemistry of Zeolites, Academic Press, 1982, p 105

[2] David, R.; Marchal, P.; Klein, J.P.; Villermaux, J.: Crystallization and Precipitation Engineering: IV − Kinetic model of adipic acid crystallization. Chem. Eng. Sci., vol. 46, 1991, 1129-1136

[3] Hounslow, M J.; Mumtaz, H.S.; Collier, A.P.; Barrick, J.P.; Bramley, A.S.: A micro-mechanical model for the rate of aggregation during precipitation from solution, Chem. Eng. Sci., vol. 56, 2001, 2543-2552

[4] Fauchadour, D.; Kolenda, F.; Rouleau, L.; Barré, L.;

Normand, L.: Peptization mechanism of boehmites used as precursors in the alumina carrier synthesis, Studies in Surf. Sci. and Catal., E. Gaigneaux eds, vol. 143, 2002, 453-461

[5] Chen, H J.; Chen, Y.W.: Hydrothermal synthesis of barium titanate, Ind. Eng. Chem. Res., vol. 42, 2003, 473-483

[6] Camp, T.R; Stein, P.C.: Velocity gradients and integral work in fluid motion, J. of Boston Society of Civil Engineers, vol. 30, 1943, 219-230

[7] Saffman, P.G.; Turner, J.S.: On the collision of drops in turbulent clouds, J. Fluid Mech., vol. 1, 1956, 16-30

[8] David, R.; Marchal, P.; Klein, J.P.; Villermaux, J.: Crystallization and Precipitation Engineering: III – A discrete formulation of the agglomeration rate of crystals in a crystallization process, Chem. Eng. Sci., vol. 46, 1991, 205-213

[9] Mersmann, A.; Braun, B.: Agglomeration, in Crystallization Technology Handbook, 2nd ed., M. Dekker, New York, 2001, 235-284

[10] Baldyga, J.; Bourne, J.: Turbulent Mixing and Chemical Reactions, John Wiley, Chichester, UK, 1999, 74-85

[11] Mersmann, A.: Crystal Growth, in Crystallization Technology Handbook, 2nd ed., M. Dekker, New York, 2001, 135-137

[12] Liew, T.G.; Barrick, J.P.; Hounslow, M J.: A micromechanical model for the rate of aggregation during precipitation from solution, Chem. Eng. Technol., vol. 26, 2003, 282-285

[13] Zauner, R.; Jones, A.G.: Determination of nucleation, growth, agglomeration and disruption kinetics from experimental precipitation data: the calcium oxalate system, Chem. Eng. Sci., vol. 55, 2000, 4219-4232

[14] David, R.; Paulaime, A.M.; Espitalier, F.; Rouleau, L.: Modelling of multiple-mechanism agglomeration in a crystallization process, Powder Technology, vol. 130 (1-3), 2003, 338-344

[15] Wachi, S.; Jones, A.G.: Dynamic modelling of particle size distribution and degree of agglomeration during precipitation, Chem. Eng. Sci., vol. 54, 1992, 3145-3147

[16] Ilievski, D.; Hounslow, M J.: Agglomeration during precipitation: II. Mechanism deduction from tracer data, AIChE J., vol. 41, 1995, 525-535

[17] Breck, D.W.: Zeolite Molecular Sieves: Structure, chemistry and use, Wiley-Interscience, 1974, 245

[18] Koegler, J.H.; van Bekkum, H.; Jansen, J.C.: growth model of oriented crystals of zeolite Si-ZSM-5, Zeolites, vol. 19, 1997, 262-269

[19] Cameirao, A.; Espitalier, F.; David, R.; Rouleau, L.: Analysis of the transformation rate from amorphous particles to crystalline zeolites Workshop on Nucleation, Saint-Etienne, France, June 17-18, 2003

[20] Schmoluchowski, M.V.: Versuch einer mathematischen Theorie der Koagulationskinetic kolloider Loesungen, Zeitschrift fuer Physikalische Chemie, vol. 92, 1917, 129-168

[21] Jacobs, P.A.; Martens, J.A.: Synthesis of high silica silico-aluminates zeolites, Studies in Surf. Sci. And Catal., vol. 33, 1987

[22] Adler, P.M.: Interaction of unequal spheres: I Hydrodynamic interaction: colloidal forces, J. Coll. Interface Sci., vol. 84, 1989, 461-474

[23] Hunter, R J.: Foundations of Colloid Science, 2nd ed., Oxford University Press, Oxford, UK, 2001, 24-32

[24] Higashitani, K.; Yamauchi, K.; Matsuno, Y.; Hosokawa, G.; Turbulent coagulation of particles dispersed in a viscous fluid, J. of Chem. Eng. Japan, vol. 16, 1983, 299-304

[25] Paulaime, A.M.: Taille et agglomération des cristaux d'une zéolithe au cours de la synthèse: effet des paramètres expérimentaux et modélisation, PhD thesis (in french), Institut National Polytechnique de Lorraine, Nancy, France, 2002

[26] Verkoeijen, D.; Pouw, G.A.; Meesters, G.M.H.; Scarlett, B.: Population balances for particulate processes – a volume approach, Chem. Eng. Sci., vol. 57, 2002, pp 2287-2303

## Author's short biography

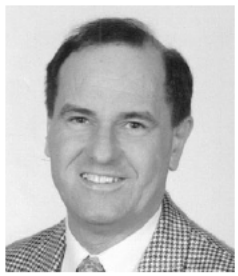

### René David

1949: Born in Pirmasens, Germany.
1968-71: Studied chemical engineering at the Ecole Nationale Supérieure des Industries Chimiques, Nancy, France.
1971-76: PhD at the Institut National Polytechnique de Lorraine, Nancy, France, on: Self-stirred reactors in the gas phase for the determination of reaction kinetics.
1976-79: Post-doc at Nancy, France, on micro-mixing effects in the liquid phase.
1979-82: Head of CNRS Office in Bonn, Germany.
1983-91: Assistant director of the Chemical Engineering Science Laboratory in Nancy, France.
Research on crystallization and precipitation engineering.
1992-98: Scientific counsellor at the French Embassies in The Hague, Netherlands, and Bonn, Germany.
Since 1998: Director of Chemical Engineering Laboratory for Particulate Solids at the Ecole des Mines d'Albi-Carmaux, France.
1999: Received the Bundesverdienstkreuz, Germany, First Class.

René David is the author of more than 80 articles in scientific journals and book chapters. He also was and still is a member of several expertise boards.

### Fabienne Espitalier

Received an engineering degree from the "Ecole Nationale Supérieure d'Ingénieurs de Génie Chimique" (Chemical Engineering Institute) of Toulouse in 1991 and a PhD degree from the "Institut National de Toulouse" on spherical crystallization in 1994. She is presently assistant professor in chemical engineering in the "Chemical Engineering Laboratory for Particulate Solids" (UMR CNRS) at the "Ecole des Mines d'Albi -Carmaux" at Albi, France. She focuses her work on crystallization and in particular on crystallization assisted by ultrasound and on spherical crystallization.

### Ana Cameirão

Ana Cameirão was born in Lisbon. She is a final-year student in chemical engineering at the Instituto Superior Tecnico of the Universidade Tecnica de Lisboa, Portugal. She is currently in her last year training at the Ecole de Mines d'Albi -Carmaux in the Centre Poudres et Procédés with Dr. R. David and Dr. Fabienne Espitalier. The subject of the training is "Improvement of mineral crystallites multiple agglomeration model in a stirred tank and computer simulation".

### Loïc Rouleau

Dr Loïc Rouleau is a research engineer in the Catalyst and Separation Division at Institut Français du Pétrole (IFP). He is in charge of zeolite development and of shaping techniques such as extrusion for refining-petrochemicals, catalysts and adsorbents. He has submitted several patents and written many articles in these fields.
Prior to joining IFP, Dr Loïc Rouleau graduated from the Engineering School in Materials Sciences in 1988 (ISITEM, Nantes) and obtained a PhD in catalysis in 1992 (Lyon).